Master of Science Thesis

Experimental Radionuclide Therapy Quantitative Pinhole planar and SPECT imaging, aiming for dosimetry based on biokinetic modeling and small animal S-values.

Fredrik Henricsson

Supervisor: Sven-Erik Strand,Lund

Department of Medical Radiation Physics
Lund University, 2005

ABSTRACT

New radionuclide therapies in humans should be preceded by experimental animal therapies, in order to evaluate the efficacy of the new therapy regime. These experimental studies have to be performed with a reliable and accurate quantification system, with properties that have been evaluated and where possible flaws have been corrected for.

The aim of this work was to evaluate the SPECT pinhole collimator high resolution imaging system to investigate the possibilities of using that imaging system as an in vivo activity quantification system in vivo in a small animal model. The pinhole collimated SPECT system used in this study was a Vision SMV DST-XL two head scintillation detector system and a lead pinhole collimator with exchangeable inserts of 3 and 1 mm pinhole diameter. The imaging system was evaluated for sensitivity, contrast, spatial resolution and countrate performance using three different phantoms, a tube phantom, a line phantom and a volume phantom. The different radionuclides used were chosen according to the different calibration measurements and according to the subsequent small animal study. The radionuclides used were ^{99m}Tc, ^{111}In and ^{177}Lu. Each of the different calibration measurements were set up with its corresponding phantom mounted on a stand in the center of the rotational axis in the camera geometry. Data acquisition was then performed during 360° detector rotation in discrete steps to obtain a complete data set for tomographic reconstruction. The acquired information was then processed with an iterative reconstruction algorithm in a computer to generate tomographic SPECT images. The reconstruction method used was a cone beam OSEM algorithm.

The pinhole SPECT investigation was then followed by an in vivo experiment utilising the knowledge from the earlier pinhole SPECT evaluation. The in vivo studies were based on a tumor model consisting of normal rats inoculated with tumor cells. The rats were injected with about 80 MBq ^{111}In / kg and about 1 GBq ^{177}Lu / kg.

The results from the pinhole SPECT studies with the line phantom showed good spatial resolution in imaging with 3 mm pinhole collimator insert with a distance between pinhole aperture and object of 28 mm. The resulting line profile through the image was analyzed, and the resolution was measured to 3.15 mm (FWHM) and the peaks from line sources separated by 4.5 mm were easily distinguished. The measured sensitivity was 3.5 cps/MBq with the 3 mm pinhole insert for ^{99m}Tc and 3.1 cps/MBq for ^{177}Lu on the central pinhole axis at a distance of mm from the pinhole aperture.

The results from the measurements of the countrate capability of the detector system showed a non-linearity in time which was surprising. Several measurements and analyses suggested this was due to a normalization procedure included in the reconstruction algorithm. This discovery led to the development of a renormalization method to allow the use of the pinhole SPECT technique as a quantification method in future measurements.

The activity quantifications in the in vivo measurements showed very good correlation with the activity measurements of the dissected tumors measured in an activity well counter.

In conclusion this study has demonstrated the feasibility of using pinhole-SPECT for quantitative in vivo imaging in small animals.

TABLE OF CONTENTS

Abstract…….....2

Introduction……...…….. 4

Material and Methods……..……6

Results…….……12

Pinhole imaging studies…….. 12

The in vivo study…….20

Discussion…… 26

Future work…….. 27

Acknowledgements…….. 28

References…...……29

Appendix ..……...31

Scintillation camera properties……31

Theory of pinhole SPECT imaging…….32

INTRODUCTION

To examine the therapeutic effect of a new radionuclide therapy procedure for patients, one should first evaluate corresponding results in a similar experimental animal therapy setup. The results must then be analyzed, calculated and used in a dosimetry model to examine and evaluate the therapeutic effect. To get quantitative results for biokinetics and radiopharmaceutical distributions, high resolution in vivo scintillation images supplemented with activity measurements of dissected organs should be performed. High resolution in vivo SPECT (single photon emission computed tomography) images can be acquired using scintillation camera system with a pinhole collimator for quantitative studies. The results can then be processed in dose calculations where small animal S-values must be used to include the effect of cross dose from long range beta particles.

Pinhole *SPECT* is a method of imaging an object in cross-sectional images (tomography) over a small field of view with high resolution. For more details on the imaging system see appendix 1. Evaluation of imaging systems based on a scintillation camera equipped with a pinhole collimator to be used in small animal studies or other examinations where a small field of view is required has been performed by several groups where the results showed good applicable use of the pinhole SPECT small structure imaging technique (S-E. Strand *et* al 1994, S-E. Strand *et al* 1993, J. Palmer *et al* 1989, B.T.A. McKee *et al* 1997, N. Schramm *et al* 2000, T. Zeniya *et al* 2004, F. Garibaldi *et al* 2004).

The purpose of this work was to examine the possibilities and the disadvantages of a scintillation camera system coupled to a pinhole collimator to be used in small animal biokinetic studies. The aim of the pinhole SPECT calibration procedure was to investigate the important SPECT imaging factors i.e. the camera spatial resolution, sensitivity, efficacy and its properties in countrate performance. It has also been shown (D. Bequé et al 2004) the importance of the imaging geometry, the source camera positions in the SPECT system, to be able to minimize the errors and artifacts in the reconstructed images, which had to be taken in consideration during the calibration measurements.

To generate the tomographic images from the sampled irradiated projections, a reconstruction program is needed. In pinhole SPECT, a FBP (filtered back projection) or an OSEM (ordered subset expectation maximization) algorithm is often used. It is important to gather a complete set of SPECT data to generate high quality tomographic images without any image artifacts, which has been shown by T. Zeniya et al 2004. A 360° rotation of the detector head round the object is often used to be able to sample the projections at many different angels and has been considered to generate a complete set of data for tomographic reconstruction. A rotation sequence of less then 360° can though be used successfully, but with a lower degree of image quality due to less sampled irradiated projections (angels). This will increase the grade of noise in the image if the number of projections is reduced.

To examine the radionuclide distributions *in vivo*, the possibility of using high resolution pinhole SPECT and pinhole planar imaging to quantitatively evaluate the activity uptake in different regions of interest was investigated. The goal in the *in vivo* study was to evaluate a procedure for small animal dosimetry based on high resolution pinhole imaging. The biokinetic modulation in pretargeting experiment combined with ECAT (*Extracorporeal Adsorption Treatment*) was studied in brown Norwegian rats. To investigate biokinetics and the distribution of the radiopharmaceutical, the study was initiated with a series of experiments where blood analysis and dissection where performed and analyzed, to generate the biokinetics in the rat. After analysis of the experiment results, a new set of experimental set ups where constructed where evaluation of immunoradiotherapy combined with the former

studies where done, with the purpose to investigate effects on tumor growth or reduction. As a complementing quantification tool in activity determination in different organs in the rat instead of dissecting and measuring in an activity counter, pinhole SPECT was thought to be an exceptional technique to use. This imaging technique would not only be of use in determine the activity content, but also a possible way of determine the geometrical activity distribution within the target area. This would be possible regarding pinhole SPECT´s properties of generating a high resolution image magnified from a small field of view. N. Schramm et al. 2000, describes a system of ultra high resolution detector system with pinhole collimator that can be used in small animal SPECT, which has an exceptional resolution and good sensitivity, and would be a promising tool to use in determination of activity distribution in small animal studies. Other groups has also shown that pinhole collimated SPECT generates excellent high resolution images over a small field of view, thus the imaging technique is well suited for small animal studies (K. Ogawa *et al* 1998, J.B. Habraken *et al* 2001).

MATERIAL & METHODS

PINHOLE IMAGING STUDIES

The camera characteristics investigated for pinhole imaging was spatial resolution, noise, sensitivity and count rate capability. The scintillation camera used was a Vision SMV DST-XL dual head scintillation camera system. The collimator used in the calibrations and the study measurements was a lead pinhole collimator with two pinhole insertions of diameters 1 and 3 mm. The radionuclides used in the different studies where ^{99m}Tc, ^{177}Lu and ^{111}In (only animal study). Energy window was set to the following parameters.

^{99m}Tc : 140 keV 20 % window
^{177}Lu : 115 keV 20 % window, 209 keV 15 % window
^{111}In (animal study) : 172 keV 20 % window, 247 keV 20 % window

The matrix size was 128×128 pixels and the pixel size was measured, according to the camera zoom, to 2.84 mm/pixel. Calibration of the scintillation camera was performed with three different types of phantoms. One designated tube-phantom was used for sensitivity and noise measurements, one line-phantom was constructed to measure the system resolution of the system and one volume-phantom was constructed to analyze the ability within the camera to keep linearity between activity and count rate over time.

The different notations in the columns of Table 1 represent the volume phantom (V), the tube phantom (T) and the line phantom (L). These phantoms are described more in detail later in this chapter.

Table 1. The measurements and its corresponding activity and phantom, in the calibration studies. L is the line phantom, T is the tube phantom and V is the volume phantom.

Measurement	Radionuclide	Phantom
Spatial Resolution	**^{99m}Tc**	**L**
Noise	**^{99m}Tc**	**T**
Sensitivity	**^{99m}Tc / ^{177}Lu**	**V**
Countrate Performance	**^{99m}Tc**	**V**

Tube phantom (T)

The tube phantom was constructed using fifteen 3 ml plastic tubes. The tube diameter was about 1.5 cm. The black marked tubes in Figure 1 were filled with 40 MBq/ml ^{99m}Tc solution and the grey tubes were filled with 20 MBq/ml ^{99m}Tc solution. The rest of the tubes were empty and were used to separate the activity sources by equal distance of 1.5 cm. The 15 plastic tubes were combined according to Figure 1 to constitute the phantom.

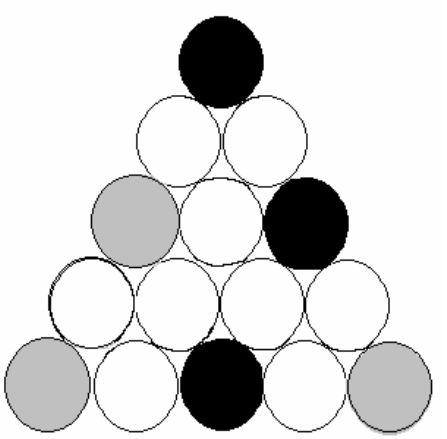

Figure 1. Tube phantom consisting of fifteen plastic tube filled with different amount of ^{99m}Tc.

Line phantom (L)

The line phantom was constructed from a plexiglass rod. The plexiglass rod was made to have about the same dimensions as a rat, with 35 mm diameter and an axial length of 80 mm.

The rod was drilled axial with 7 equally spaced parallel holes. Each hole was 2.5 mm in diameter and was drilled with 2 mm space between them. The phantom can be seen in Figure 2.

In these holes a capillary of 700 mm of total length and a diameter of 2 mm was inserted which was filled with a total activity of about 100 MBq ^{99m}Tc solution. Thus there was an activity concentration of 81 MBq/ml and 1.2 MBq/cm.

Figure 2. Line phantom with parallel channels to be filled with activity solution

Volume phantom (V)

The volume phantom was constructed from six identical plastic boxes, attached together into a large box as in Figure 3a and 3b. Each box measures 14×24×24 mm^3. These plastic boxes are hollow and able to be filled with approximately 4 ml of activity solution.

In the countrate performance study, the volumes were filled with different amounts of ^{99m}Tc activity in each 4 ml boxes, as given in table 2.

Box	Activity (MBq)
1	**300**
2	**250**
3	**200**
4	**150**
5	**100**
6	**50**

Table 2. Activity of ^{99m}Tc In the different phantom boxes

Figure 3a. Volume phantom with boxes attached according to figure 3b.

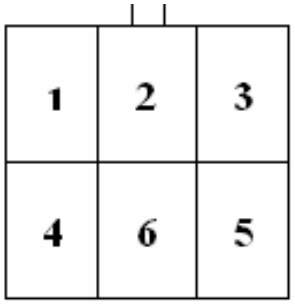

Figure 3b. Box position in the volume phantom

The different phantoms were constructed in such small dimensions to fit the rat fixation tube. This plexiglass tube was to be mounted on an experimental stand constructed to fit the SPECT imaging setup with the rotating two head scintillation camera system. The experimental setup with the rat fixation plexiglass tube is shown in Figure 4.

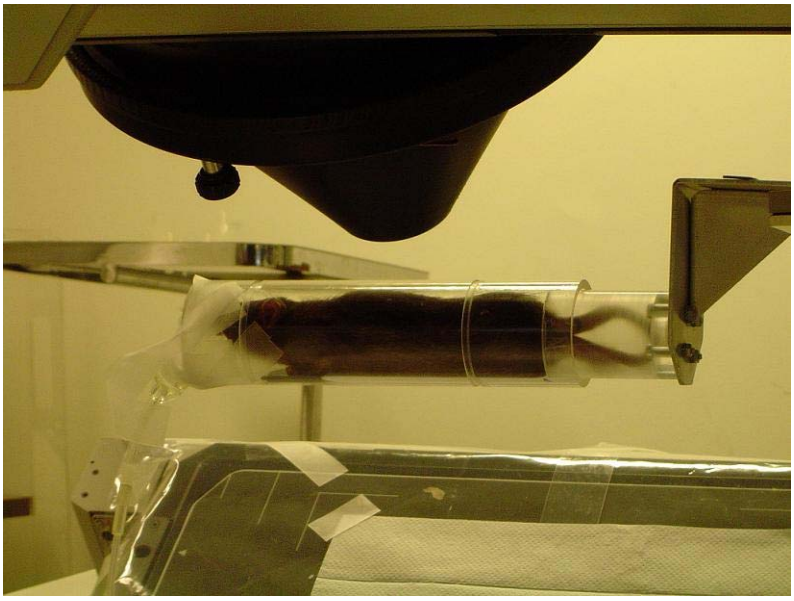

Figure 4. Experimental rat fixation tube with a rat positioned for pinhole SPECT imaging

The scintillation camera was set up with the following parameters during the tests to define the experimental setup geometry for the reconstruction program. The pinhole crystal distance (a, see figure 1 in appendix) was 302 mm, distance between crystal surface on the camera heads, measured to 638 mm, and indicated radius after parking of the gantry (starting position) was 280 mm. When calibrating for SPECT, 2 different pinhole diameters were tested, 1 mm and 3 mm. The projection angles where set to (360/128)° per angle, and the sampling times varied between 10 to 30 s per angle.

The reconstruction program used in the pinhole SPECT studies was a cone beam OSEM reconstruction algorithm. This is an algorithm used for cone beam computer tomography in pinhole SPECT.

No scatter or attenuation corrections were made in this study.

COUNTRATE CHARACTERISTICS

To investigate the countrate characteristics of the pinhole SPECT system the volume phantom was filled with ^{99m}Tc in the different boxes with activity content according to Table 2 and Figure 3b. The boxes were filled with different, known amounts of activity to state the countrate abilities and possible camera countrate abnormalities in both high activity regions as in low activity regions. The volume phantom was mounted on a stand positioned in origo of the SPECT rotation geometry, COR[i], in the camera. The 3 mm diameter pinhole insert was used with a radial distance between pinhole and object (b, see figure 1, appendix 1) of 28 mm. The sampling procedure used was a step-and-shoot procedure where the number of projection angles was 128 in 360° total sampling rotation. Sampling time per angle was set to 10 sec. The sampled projections were then processed in the OSEM reconstruction algorithm to generate tomographic images.

When investigating the countrate characteristics of the camera, the results showed an abnormal behavior in the reconstruction algorithm which had to be taken in consideration. The reconstruction problem in renormalization of the tomographic images had to be solved, and a normalization method in re-calculating the images was developed.

The normalization factor was calculated by dividing the sum of the total counts in all projections with the sum of the total counts in all tomographic images, according to Equation 1.

$$\frac{\sum \tau}{\sum \pi} = \kappa \qquad (1)$$

In Equation 1, τ denotes count rate density in the tomographic ROI, π denotes count rate density in the projection ROI and κ is the normalization factor. Both ROI´s are set to confine the whole phantom in the study.

IN VIVO TUMOR BIOKINETIC PINHOLE SPECT MEASUREMENTS

One study for diagnostic purposes was performed. The radionuclide used was ^{111}In, a radionuclide with a physical halflife of 2.8 days. In this study a rat was SPECT imaged 6 hours post injection of Streptavidin-^{111}In to analyze the activity uptake, the possibility of determination of tumor size and the geometrical activity distribution in the tumor. The results from this measurement were then to be compared with measurements of the dissected tumor.

The second study was a radioimmunotherapy study where ^{177}Lu-Streptavidin was injected in rat after pretargeting with the antibody BR96-1033. ^{177}Lu is a radionuclide with a physical half-life of 6.7 days and a β maximum energy of 498.3 keV (I (%) = 78.6). A set of measurement series of pinhole SPECT imaging was setup to investigate the possibility of generating quantitative information of the activity distribution in regions of interest. The results of these measurements were then to be compared to biokinetic information obtained

[i] COR - Center of rotation

from activity measurements of dissected organs and tissues. To sample information to generate the biokinetics, blood sampling and planar scintillation imaging was performed at 3, 6, 9, 12 and 24 hours post injection of Streptavidin-^{177}Lu. To be able to verify the absolute activity content of different tissues, the animals were dissected at times illustrated in Figure 5. These results from activity quantification from dissections were later to be compared with measurements with the pinhole SPECT imaging. The rats were imaged with pinhole SPECT 5 times through 7 days. First imaging procedure was 6 hours 57 min post injection, second 19 hours 37 min p.i., third 27 hours 2 min. p.i., fourth 68 hours 30 min p.i. and fifth 164 hours 45 min. p.i. This procedure is illustrated in Figure 5. Every projection time was set to 15 seconds and every rotation angle was set to 360/128 degrees.

The *in vivo* model being used was BN rats inoculated with BN7005 rat colon carcinoma cells. Pretargeting with antibody BR96 coupled to the molecule 1033 was performed. The rats were intravenously injected with DOTA-Streptavidin labeled with ^{111}In and ^{177}Lu. Extra corporeal adsorption treatment (ECAT) was performed using a pump with a set of capillaries surgically operated into the rat artery and vein and attached to a filter column, to be able to filtrate the blood plasma from circulating not targeted antibody.

To perform the biokinetic study with pinhole SPECT imaging, Vision SNV DST-XL dual head scintillation camera system with pinhole collimator was used with adjustments according to prior calibration measurements. The time points of the experimental therapy set up were performed according to Figure 5.

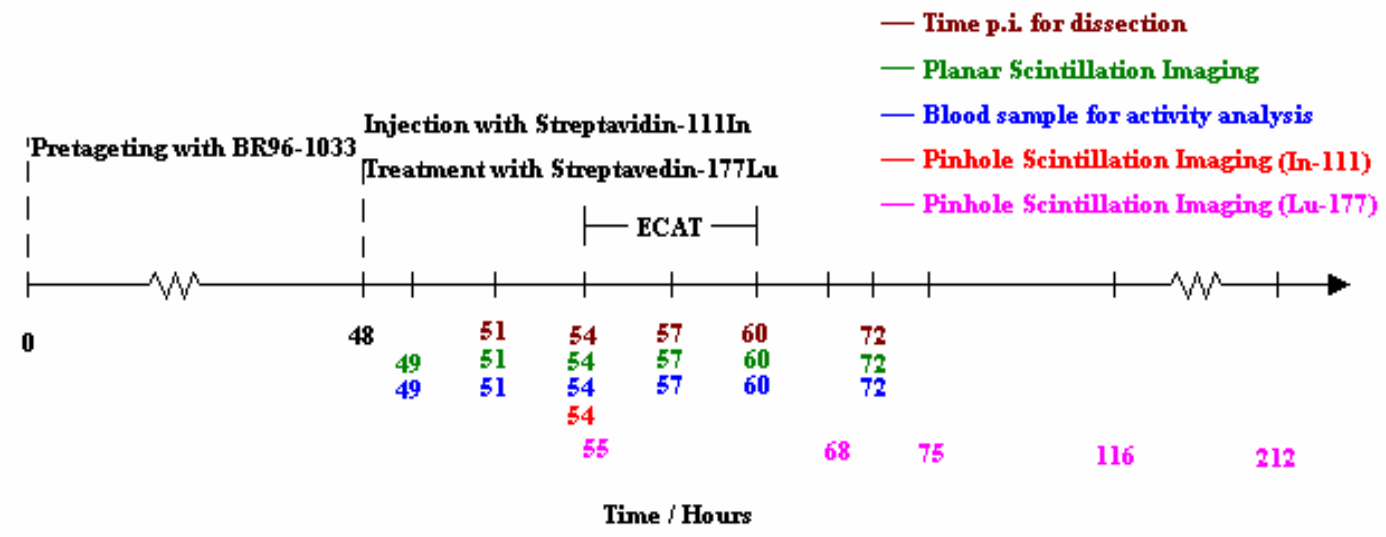

Figure 5. Illustrated timescale of the experimental radionuclide treatment therapy study

RESULTS

PINHOLE IMAGING STUDIES

Measurement of SPECT noise

The noise was measured with the tube phantom. The reconstructed tomographic images from the pinhole SPECT measurements with the tube phantom are shown in Figure 6.

A line profile of the signal (countrate) variation over two different tubes (Hi/Low activity content) has been applied. This was made according to Figure 6.

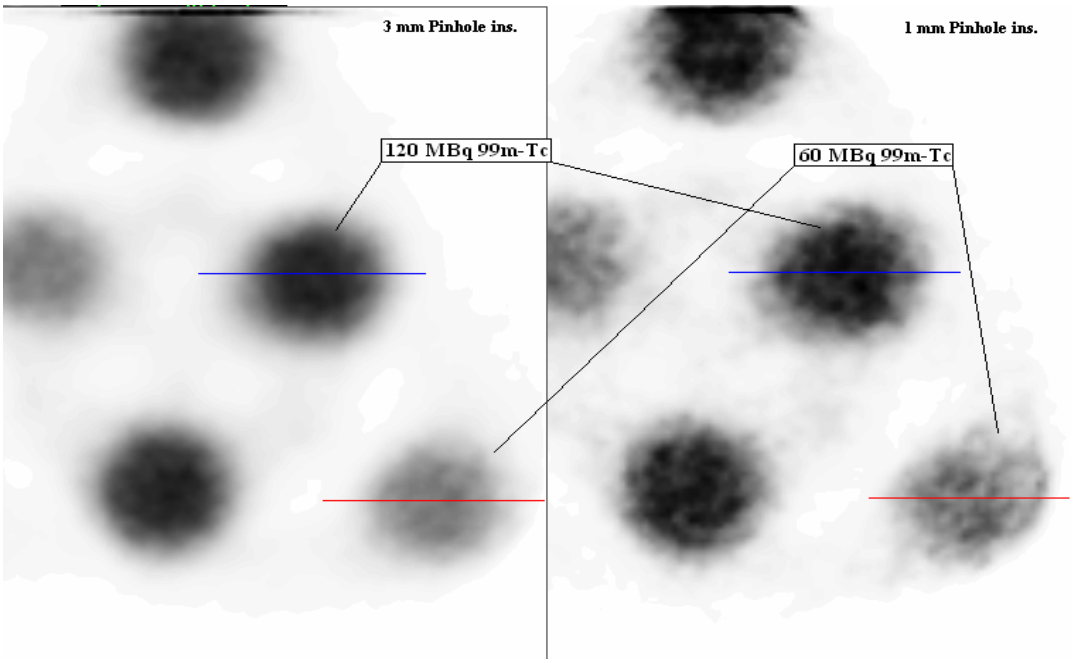

Figure 6. Illustration of the line profiles drawn through hi- and low- activity tubes in the tomographic images. Left imaged with the 3 mm pinhole insertion and right imaged with 1 mm pinhole insertion.

It is shown in Figures 7 - 10 that there is a less degree of count variation in the phantom imaged with 3 mm pinhole diameter. Figures 7 and 8 are line profiles of the tube phantom, applied according to Figure 6, imaged with the 3 mm pinhole insertion. The line profiles in Figures 7 and 8 shows a smooth profile shape with a less degree of count/pixel variation (noise), relative the images imaged with the 1 mm pinhole diameter. The line profiles in Figures 9 and 10 shows a more irregular shape of the profile and a higher variation of the count/pixel values within the tubes. This is due to a higher degree of noise in the tomographic images generated from imaging with 1 mm pinhole diameter.

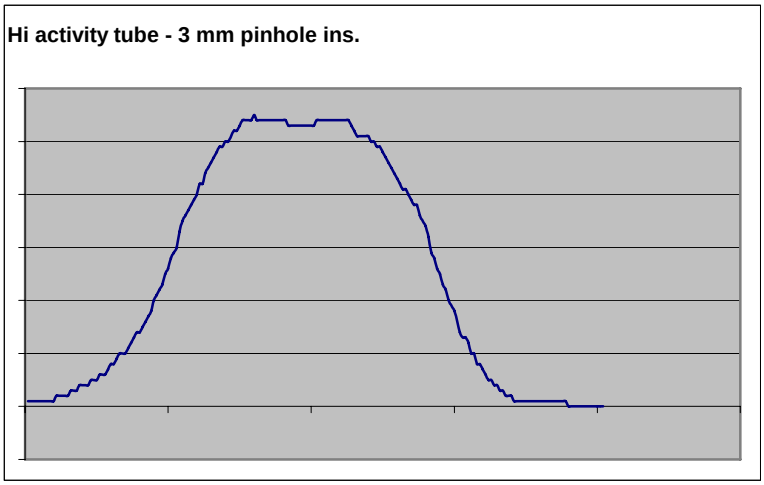

Figure 7. Line profile of the count/pixel variation through the reconstructed image according to Figure 7. Line profile of the high activity tube imaged with 3 mm pinhole insertion

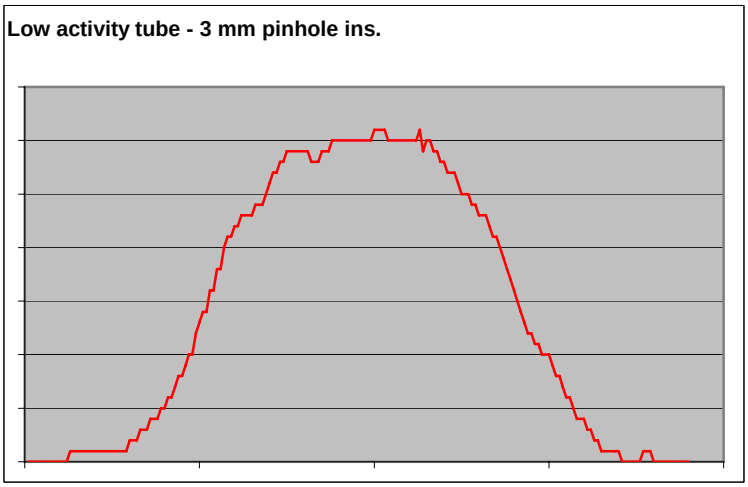

Figure 8. Line profile of the count/pixel variation through the reconstructed image according to Figure 7. Line profile of the low activity tube imaged with 3 mm pinhole insertion.

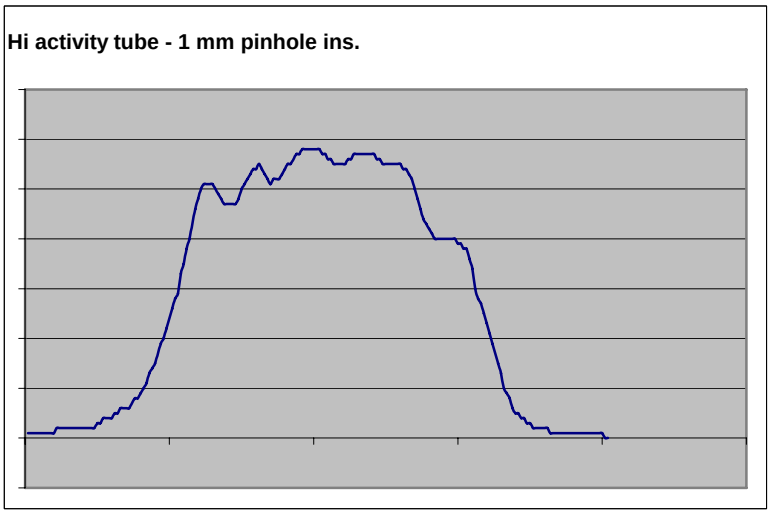

Figure 9. Line profile of the count/pixel variation through the reconstructed image according to Figure 7. Line profile of the high activity tube imaged with 1 mm pinhole insertion

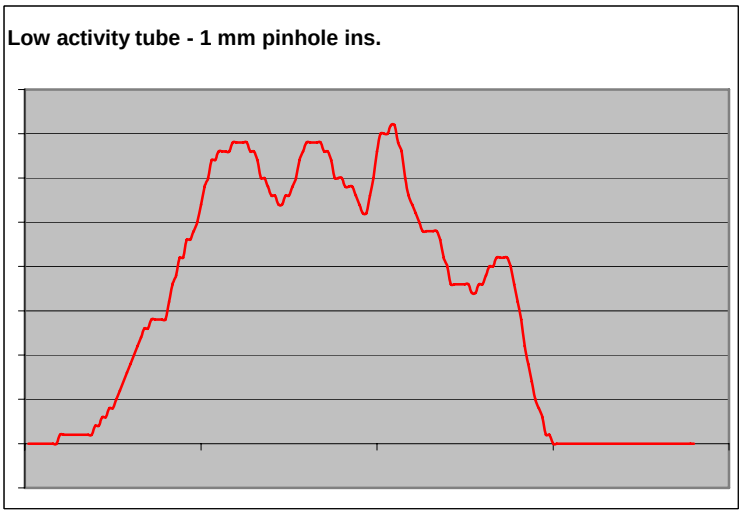

Figure 10. Line profile of the count/pixel variation through the reconstructed image according to Figure 7. Line profile of the low activity tube imaged with 1 mm pinhole insertion.

The 3 mm. pinhole collimator insertion was chosen for further studies because of the lower noise. From the results of measured line profile and as seen in figure 6, the image quality (according to noise reduction) was sufficient better as the 3 mm pinhole insertion was used.

Measurement of camera sensitivity

The pinhole SPECT camera sensitivity was measured with the volume phantom. The box cavities were filled with a known amount of activity and was imaged in origo of camera SPECT geometry, COR (center of rotation). The object was imaged with a fix indicated radial detector head distance of 340 mm and a pinhole diameter of 3 mm. The phantom was imaged accordingly, and with knowledge of activity content in phantom and the corresponding countrate from the images, the sensitivity was calculated.

Pinhole SPECT Camera sensitivity measured with ^{99m}Tc and ^{177}Lu: 3.5 cps/MBq (^{99m}Tc)
3.1 cps/MBq (^{177}Lu)

Measurement of spatial resolution

The study of the spatial resolution was performed using an activity concentration of 81 MBq/ml ^{99m}Tc in the line phantom. The scintillation camera was able to resolve small structures as 1 mm, as seen in figure 11, which was very easily visualized as separate capillaries in the reconstructed tomographic images. With knowledge of former measurements on the countrate variation through a SPECT image of the phantom, it was decided, according to the noise, to only use 3 mm aperture in further measurements. These measurements were made with pinhole diameter of 3 mm and with an indicated radial detector head distance of 340 mm.
The results from these measurements are shown in figure 11 and 12.

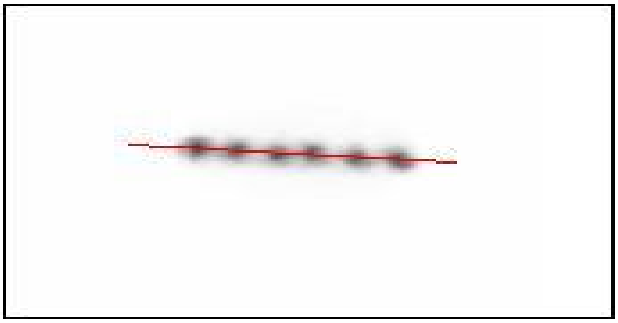

Figure 11. Reconstruction of the line phantom. The center of the capillaries are spaced equally in intervals of 5 mm, with inner and outer diameters of 1 mm and 2 mm.

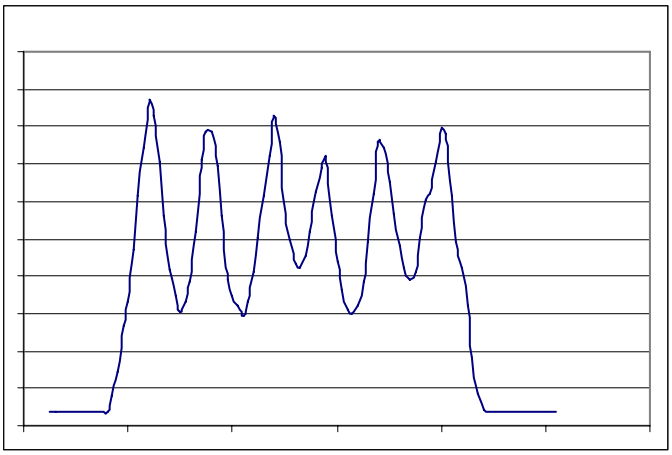

Figure 12. The line profile according to the line drawn in figure 8, showing the count/pixel variation through the reconstructed image. The FWHM is 3.2 mm.

The results from the analysis of the count per pixel line profile can easily be separated as individual peaks. The "*full width at half maximum"* (FWHM) is measured to be approximately 3.2 mm. Analyzing Figures 7-10, it can be discovered that 1 mm aperture was generating higher resolution images, but with further study, it was decided to use the 3 mm aperture regarding the high noise and the irregular shape of the image profiles generated by the 1 mm aperture.

The 3 mm pinhole diameter was discovered to generate high resolution, low noise and good contrasts of the tomographic images, and the used radial detector head distance was enough to generate images of useful FOV to get the enlargement of the capillaries.

Measurement of camera count rate statistics

The reconstructed images from the volume phantom (Figure 13) showed very good visual image quality.

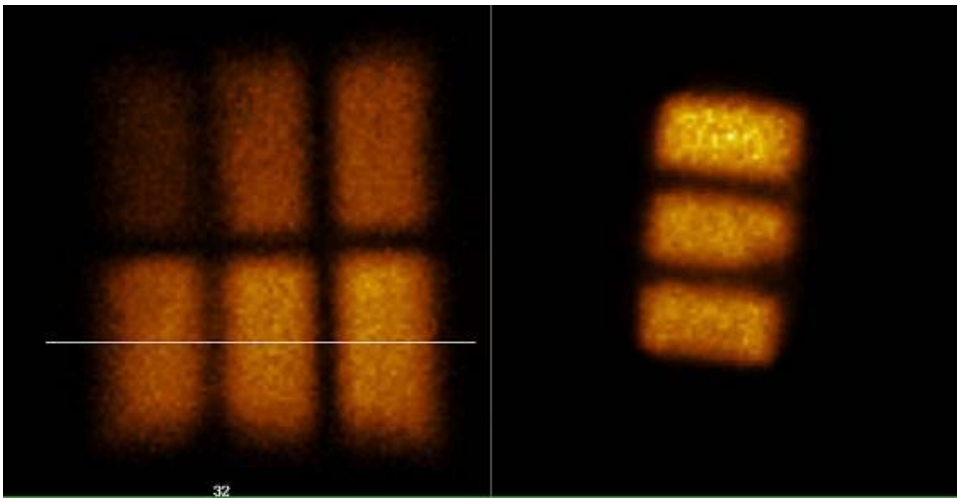

Figure 13. Planar pinhole projection image (left), and the tomographic image reconstructed approximately from information from the transversal slice indicated by the white line

As they were imaged with constant time intervals, it was expected that the count rate density within the picture matrices would follow an exponential decay. With identical ROI measurements during the image series, it was discovered that the countrate density, which is directly related to the activity, in the reconstructed images did not follow that relationship. The relation between measured countrate density in ROI´s and corresponding activity is shown in Figure 14, where the blue line is the measured countrate density and the red line is the expected "normal behavior" of the countrate density.

This phenomenon was then further investigated in different measurements where the measured countrate as function of time was studied. The results showed that the reconstructed images were never correlated to an exponential decay relationship.

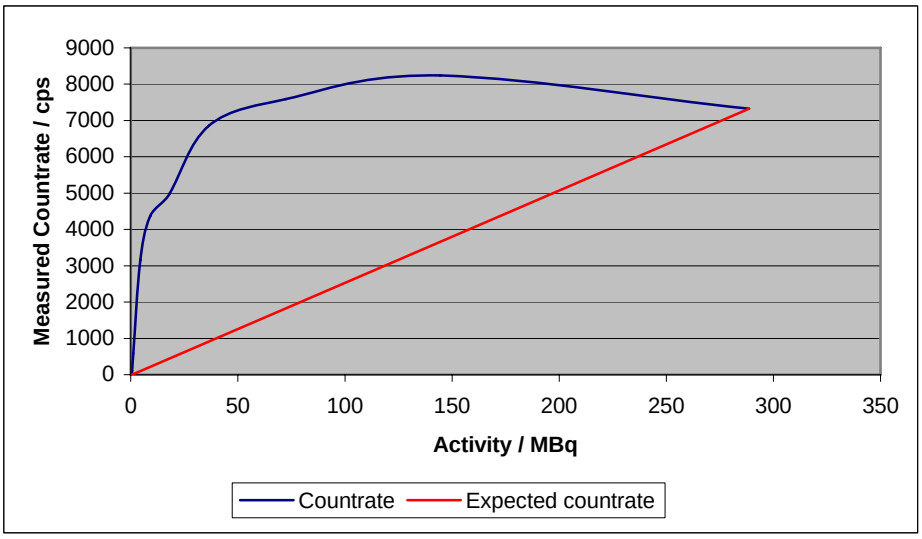

Figure 14. Measured ROI countrate density in series of tomographic images as function of corresponding activity and the expected behavior of the graph.

In Figure 15, the result of the effect of the renormalization in the reconstruction algorithm can be seen. The reconstruction program has generated different normalization factors at different time points to scale the images with. (for more details see discussion). In Figure 15, the normalization effect results in that the count rate relation has a high positive gradient at the first hours, which then tend to decrease to negative values at later time. These results are not expected as the count rate-activity relation should be linear.

After identification of the reconstruction problem, the information of projections and reconstructed tomographic images were gathered, to compare the differences. The calculation procedure had to be done for all the measurements, if a quantification of the signal content in the tomographic images was to be studied. The calculations were made according to Equation 1. If the normalization factors are used for all the reconstructed images, the "true" countrate for every tomographic slice can be created as it would appear if the reconstruction algorithm was correct from the beginning. The results of a corrected countrate in a tomographic image (with activity content) are shown in Figure 17. In Figure 15 the activity content in the tomographic image # 50[ii] corresponds to about 750 MBq at time t = 0 and the activity content in the tomographic image # 80[iii] corresponds to 200 MBq at time t = 0.

After correcting the measured count rates, the results in Figure 18 were obtained and a linear relationship between measured countrate and activity was found.

[ii] Notation of a tomographic slice with high activity content, see Figures 15, 17 and 18
[iii] Notation of a tomographic slice with low activity content, see Figures 15, 17 and 18

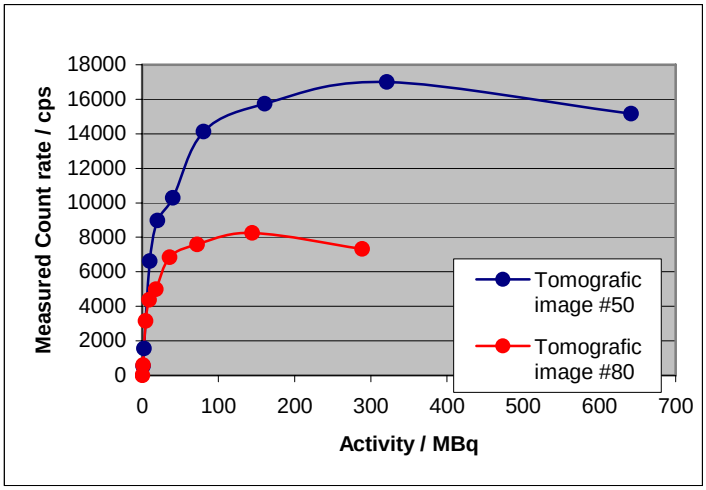

Figure 15.Uncorrected measured countrate as a function of activity in two reconstructed slices

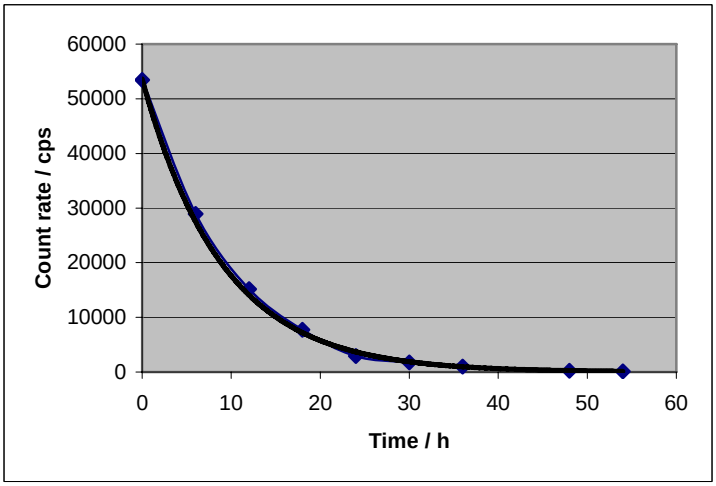

Figure 16. The sum of counts in total number of projections as a function of time. Also show the theoretical exponential decay relaxation

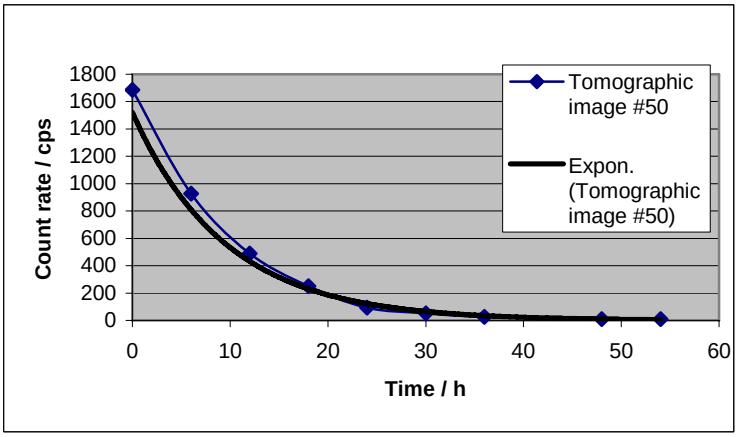

Figure 17. Corrected countrate within a ROI in a tomographic image as a function of time. Also show the theoretical exponential decay relaxation

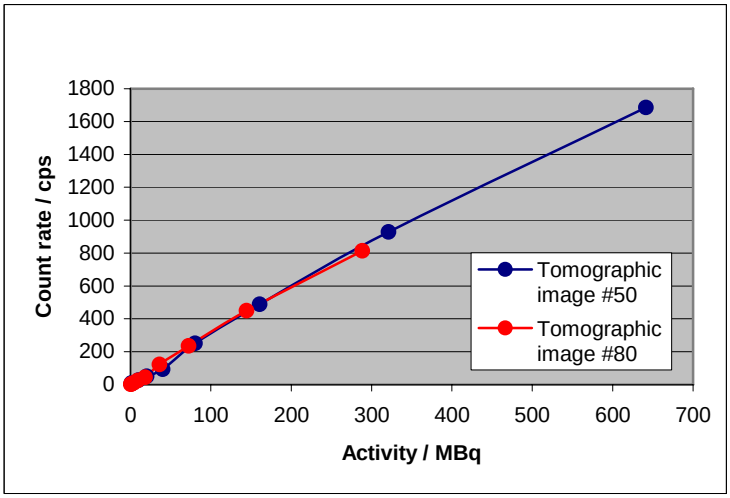

Figure 18. The camera count rate capability after correction. The blue line corresponds to measurements of the high activity phantom (750 MBq ^{99m}Tc). The red line corresponds to measurements of the low activity phantom (300 MBq ^{99m}Tc).

THE IN VIVO STUDY

The diagnostic study

The initial studies performed, to verify biokinetic theories of radiolabeled tracer uptake, were in diagnostic purpose and were subject to a smaller amount injected activity of ^{111}In. The radionuclides were coupled to a molecule called *Streptavidin* to be post injected into the body after pretargeting the tumor cells with injected antibodies. The activity distribution of ^{111}In in the body can explicitly be studied in the planar scintillation image in Figure 20.

In Figure 19 it may be possible to visual determine an activity uptake. In Figure 19 we can see high concentration of activity in radiolabeled streptavidin combined with the antibody conjugate, mostly free in blood plasma in blood rich organs of the body. In this particular case it is even possible to determine the uptake in tumor and the position of the tumor, located lateral of *columna spinalis* on the right side. Using the pinhole SPECT technology to generate a high resolution small field of view image, the results shown in Figure 20 are obtained. In Figure 20 the tomographic image of the tumor shows a greatly enhanced possibility to quantify the activity uptake and even the geometrical distribution of the radiolabeled antibodies within the tumor volume of interest. With knowledge of the zoom factor in the camera which was set to 2.84 mm/pixel, the tumor in the tomographic image was calculated to be 112 mm in diameter, which could be verified after measurement of the true spatial geometry of the dissected tumor. The results are illustrated with a ruler that measures the tumor size at top of Figure 20.

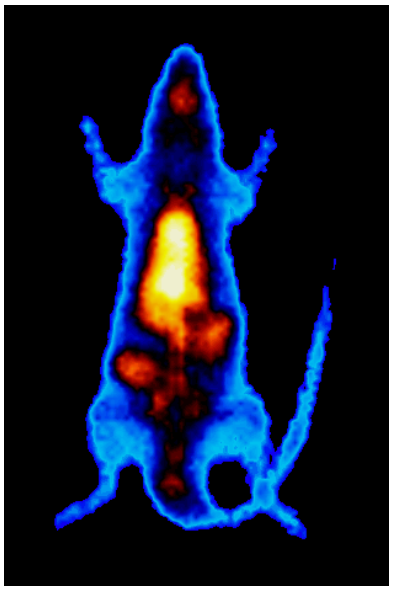

Figure 19.Planar image of a rat injected with BR96-1033 + ^{111}In-Streptavidin. In the image can be seen activity uptake in the tumor and activity in blood rich organs.

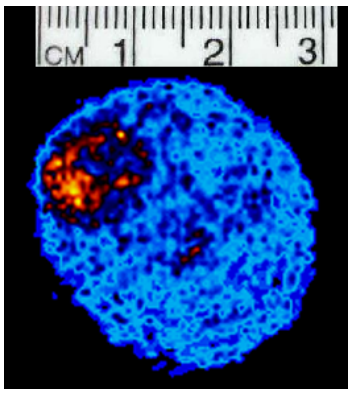

Figure 20. Pinhole SPECT of the rat in Fig. 19.

The therapy study

To verify tumor size and activity uptake in region of interest, a planar scintillation image was taken after every blood sample time points (see Figure 5). The result of sampled images from parallel hole and pinhole collimated scintillation camera imaging is shown in Figure 21. An example of the difference in resolution and the magnification effect between parallel hole collimated imaging and pinhole collimated scintillation imaging can be seen in Figure 21.

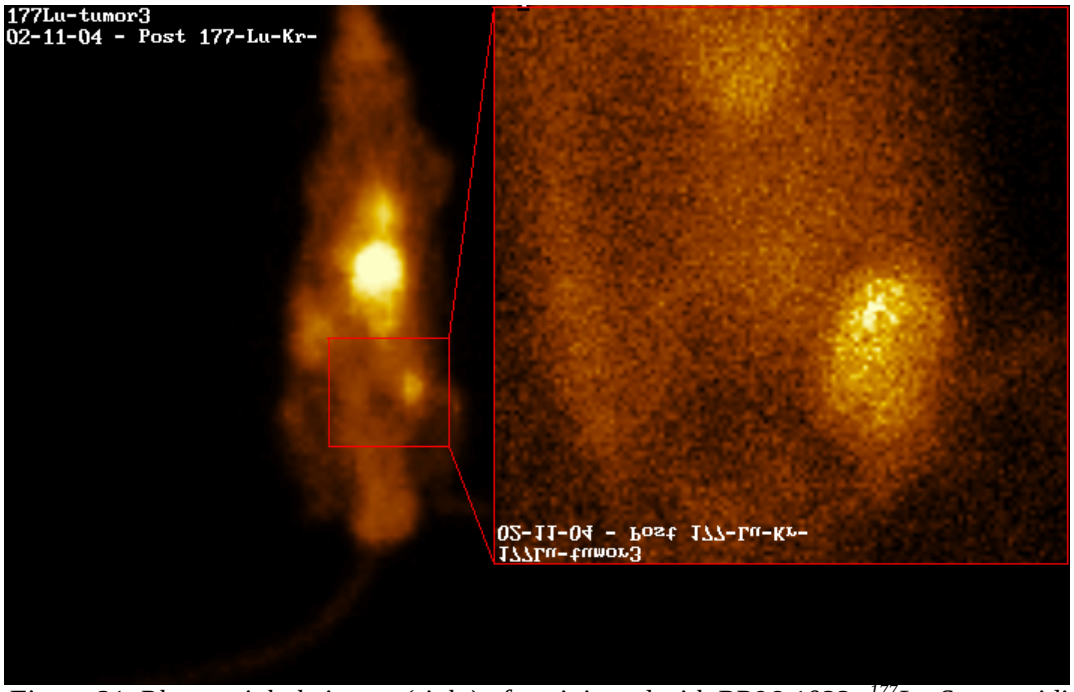

Figure 21. Planar pinhole image (right) of rat injected with BR96-1033+^{177}Lu-Streptavidin

The results of the pinhole SPECT imaging of the rat with the inoculated tumor are shown as reconstructed tomographic images in Figure 22. The image series in Figure 22 are the reconstructed image from approximately the same transversal slice in the examinated rat volume, at different time points.

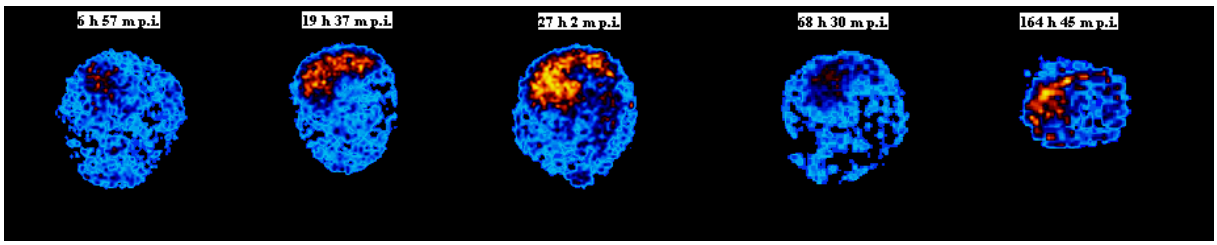

Figure 22. A series of same tumor in rat, pinhole SPECT imaged after different time intervals post injection. ^{177}Lu injected in Rat.

A ROI was made around the tumor area in the images in Figure 22, to estimate the count density and to quantify the activity content in the tumor, at different times post injection of the radioactivity. The information of count density in the different ROI´s was correlated to true activity content obtained from dissection of tumors.

Analyze of number of counts in the ROI´s in the different images in Figure 22 revealed a countrate according to the numbers in Table 2 at the different measurement points. These count rates were then corrected for matrix renormalization according to the method developed in earlier described renormalization problem (Equation 1).

The result from the renormalization correction must then be corrected for physical decay. This was made according to equation 2, where N is the measured countrate and N_0 is the countrate corrected for physical decay.

$$N_0 = \frac{N}{e^{-\frac{\ln 2}{T_{1/2}} \cdot t}} \qquad (2)$$

1			Sampled data (uncorrected values)			
	Measurement	TIME	TIME post inj. (h)	Count rate / cpm		
	1	041101 15:30	0	0		
	2	041101 22:27	6,95	9223,97		
	3	041102 11:07	19,62	35153,78		
	4	041102 18:32	27,03	60392,25		
	5	041104 12:00	68,5	21963,13		
	6	041108 12:15	164,75	4637,41		
		Sum of ROI in tomo images	Sum of ROI in projections	Normalization factor	Corrected for matrix renormalization	Corrected for decay
		$\Sigma\tau$	$\Sigma\pi$	κ	τ	τ
2	Measurement	# of counts	# of counts		Count rate / cpm	Count rate / cpm
	1	0	0	0	0	0
	2	70634086	1334520	52,9	174,2	179,5
	3	156628704	1768636	88,5	396,9	431,9
	4	301463952	1885788	159,8	377,7	424,4
	5	112270400	1314442	85,4	257,1	359,6
	6	22683769	682941	33,2	139,6	284,0

Table 2. Calculated results from count rate determination in ROI from pinhole SPECT images of tumor in rat, injected with ^{177}Lu.The sampled countrate density is corrected for reconstruction matrix renormalization and physical decay.

The results of the determination of activity content in the tumor at different times post injection, is shown in Figures 23, 24 and 25. Figure 23 shows the uncorrected values as measured directly from the resulting reconstructed images in the measurement series. In Figure 24, the data points are corrected for the matrix renormalization according to the correction method. Figure 24 illustrates the effective halflife of the investigated radiopharmaceutical. Figure 25 shows the results after correction of the physical halflife of the radionuclide, thus it shows the biokinetics.

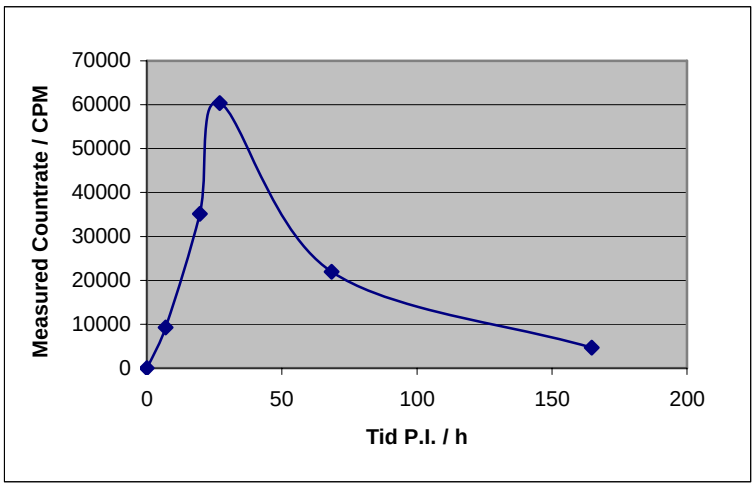

Figure 23. Measured countrate in tumor ROI as a function of time

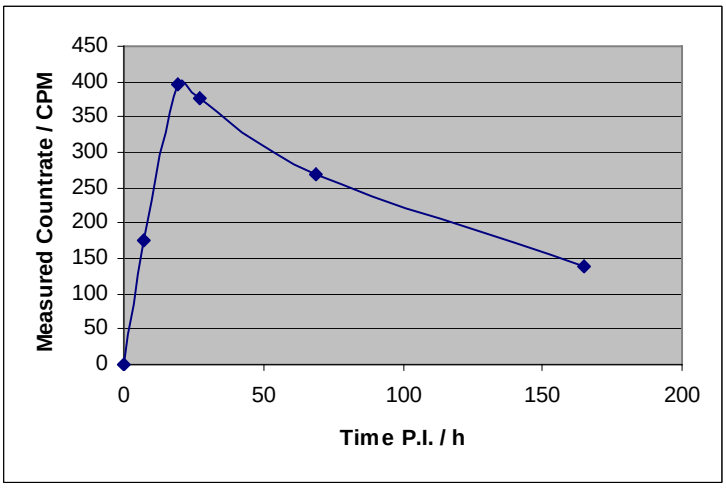

Figure 24. Measured countrate in tumor ROI corrected for matrix renormalization

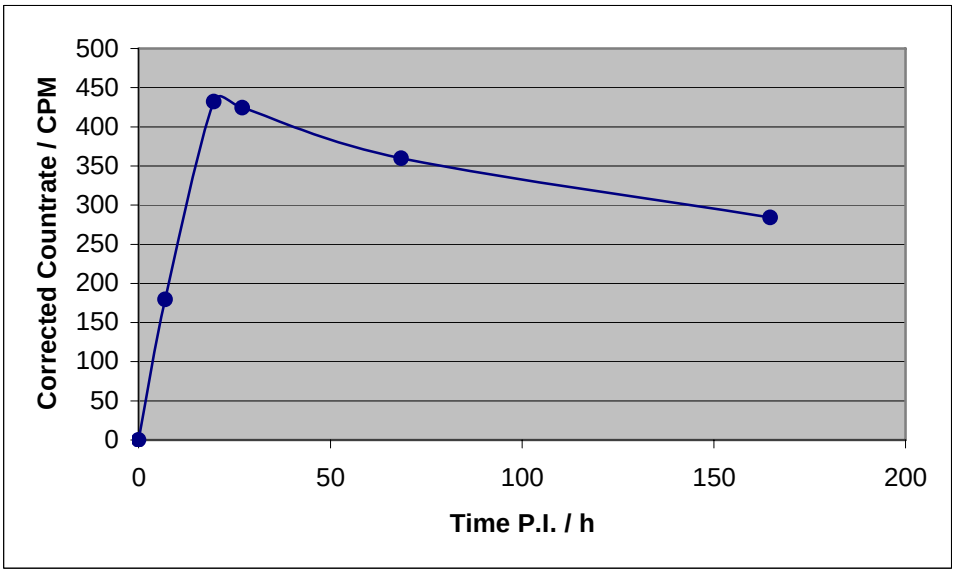

Figure 25. Measured countrate in tumor ROI corrected for matrix renormalization and physical decay

In Figure 26 the data of activity content in tumor generated from information in tomographic pinhole SPECT images is compared with data from absolute measured activity content in dissected tumors, measured in a well type detector (activity counter). The measured corrected countrate data point from the pinhole SPECT images has been converted to tumor activity uptake in percent injected activity per gram tumor tissue. This was calculated from the corrected data points in Figure 25, which were received with knowledge of the measured calibration factor, which describes the relation between the measured countrate according to the present activity content. The calibration factor was calculated by an arithmetic mean of the slope of the relation in Figure 18. The calibration factor used was 3.3 cps/MBq. In the specific activity calculations, the rat tumor weight was determined to be approximately 1 gram, which in reality varied about ± 0.2 gram between the rats. The injected amount activity solution in the rat was 1 GBq ^{177}Lu/kg. The % I.D. /g could then be calculated by the ratio of the measured SPECT ROI content in cps/Mbq, of the tumor, and the calibration factor. This ratio was then divided by the injected amount of activity per gram to receive the % I.D. /g. These calculations were made to be able to compare the measurements with data from dissected tumors.

The results are shown in Table 3. The comparison between the pinhole SPECT imaging study and the received results from measurements of dissected tumors is shown in Figure 26.

	^{177}Lu-BR96-1033 Calculated from P-SPECT	^{111}Lu-BR96-1033 Calculated from dissected tumors
TID post inj. (h)	**Tumor uptake % I.D./g**	**Tumor uptake % I.D./g**
0	0	0
1.5		0.6
7	0.95	
8		1.2
19.5	2.20	
24		2.3
27	2.15	
48		2.0
68.5	1.85	
96		2.1
165	1.45	

Table 3. Results from calculating specific activity in tumor in P-SPECT images and compare with measurements of dissected tumors.

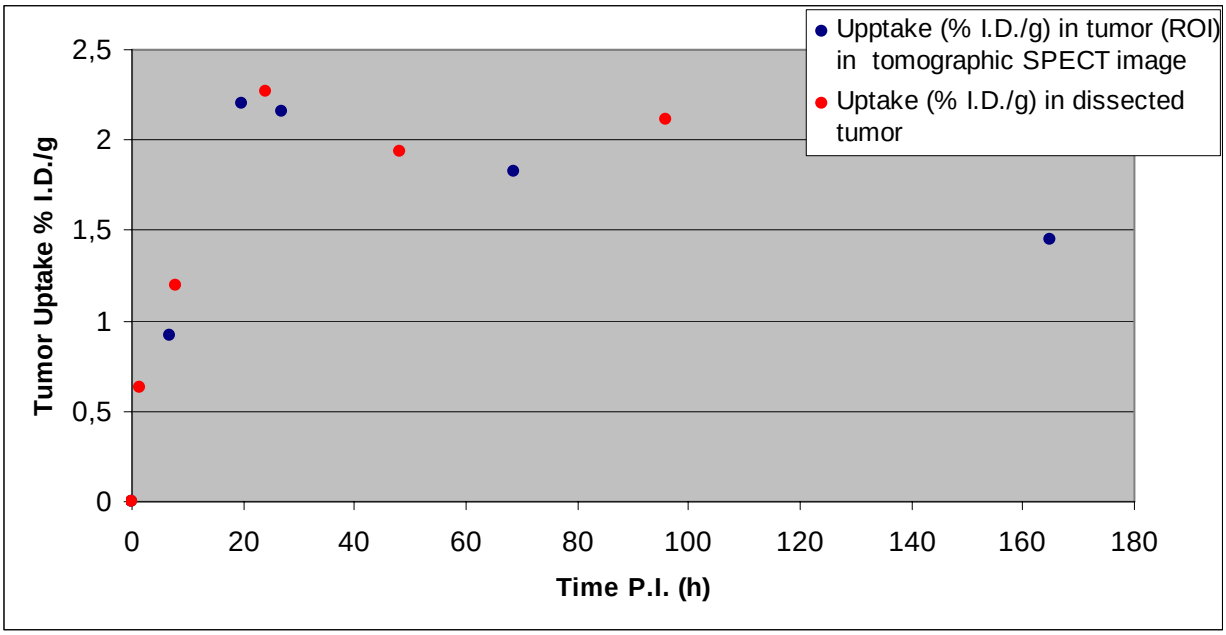

Figure 26. Correlation between measured and calculated uptake in tumor ROI in tomographic P-SPECT images and measured activity content in dissected tumors[iv].

[iv] A mean value of three different animals was used on the data points.

DISCUSSION

Pinhole SPECT imaging in small animal studies has been evaluated and verified to be of great value by many research groups (S-E. Strand *et al* 1994, K. Ishizu *et al* 1995, J.B. Habraken *et al* 2001). This technology has potential of generating very high resolution tomographic images over a small field-of-view, which is very desirable in small animal studies. This work has shown that a proper evaluation of the pinhole SPECT camera system must be performed if the imaging system is going to be used in i.e. biokinetic and dosimetry models, where organ uptake and activity quantification is of great importance for the study. In this work, a use of the pinhole SPECT imaging system as an activity quantification system without proper investigation of the SPECT camera imaging system properties, could have been misleading in the following *in vivo* studies. Because of the abnormal behaviour in the reconstruction algorithm, a analyze of the generated tomographic images would give wrong activity content, relative the actual activity content, in the target organ, which would complicate future dosimetry calculations. By investigating the pinhole SPECT camera it is possible to develop a correction method when the problem has been identified. When the correction calculations has been applied in the imaging process, the pinhole SPECT camera is a reliable and very useful imaging tool to use in further *in vivo* studies. In this work, the camera countrate problem had to be considered and investigated.

THE COUNTRATE PROBLEM

At first, the scintillation camera properties of imaging at high countrate were thought of being the main problem after investigation of the dysfunctional countrate behavior in the reconstructed SPECT images. About 1 GBq of total ^{99m}Tc activity was used in the volume phantom, which could be a problem with deadtime and pileup effects within the camera system. After consulting documents on the Vision SNV DST-XL scintillation camera, it was believed that the scintillation camera should not have any difficulties of imaging at the present countrate. When the gathered projections alone were examined, they showed as expected, an exponential decay relation. Further investigation suggested possible problems with the reconstruction algorithm. These problems were suggested with the knowledge of expected results from the projections and the strange behavior in pixel values of the reconstructed tomographic images. Studies of the signal variation in the image matrices led to believe that the reconstruction algorithm had a build in function to renormalize every pixel values in all image matrices of the reconstruction. A probable theory of the renormalization problem in the reconstruction program was discovered. The iterative processes which are governed by the reconstruction algorithm are generating a reconstruction volume in three dimensions, V(x,y,z), in which the results from the calculation processes are stored. These iterative calculations, in this case OSEM, are products of a three dimensional pixelcount function and a multi dimensional probability function, which depends on the constructed volume geometry and the collected projection characteristics. How the functions are exactly implemented and operating in OSEM is not known. The computer workstation program is set to work with 16 bit max information per pixel. However, the true usage of every pixel is only 15 bit, hence the maximum pixel value is 32677 (0-32677). It seems that the reconstruction program in every way normalizes the iterative functions as it should in different measurement situations and different geometries, but it chooses to scale the generated results (voxels) with a value to get as good numerical dynamic proportion within the image matrix as possible. This process function in the reconstruction algorithm is hard to fully understand, because of the lack of generated information from the program after a reconstruction process.

Analysis of results from the fact that the reconstruction algorithm scales the image matrix values by the highest image pixel value in the image series to generate a matrix with good numerical dynamic within the image series, suggests the algorithm to work accordingly to enhance the image qualities. This knowledge must be advised at every measurement with pinhole SPECT imaging if quantification of activity content in the reconstructed images is to be made accurately.

FUTURE WORK

The collected data from the analyses of the reconstructed tomographic images in the small animal studies are later to be used in dosimetry calculations to evaluate the therapeutic effect in the radio immunotherapy model. To use the data from the study in a dosimetry model, the data are to be analyzed in a compartment model to calculate the cumulated activity in the organs of interest. The results of the calculations are then combined with generated specific small animal S-values, to calculate the dose distribution in the body. For this purpose, “small animal dosimetry” is needed.

The obtained biokinetic data from the pinhole SPECT studies can be used for further calculation of the absorbed dose for tumors and tissues. The so called “small animal dosimetry” must then be applied.

The average absorbed dose in an organ or tissue is described by equation 3 (13).

$$\overline{D}_k = \sum_h \tilde{A}_h \times S(k \leftarrow h) \qquad (3)$$

The cumulated activity, $\tilde{A}_h$, describes the total amount of decays in the source organ (h), where k is the target volume. The S-value describes the physical characteristics such as energy and type of radiation, dimensions of the source region and the composition of the medium in the source region. The cumulated activity is calculated by an infinite integral of the activity uptake and effective decay of the region of interest as described in equation 4.

$$\tilde{A} = \int_0^\infty A(t)\partial t \qquad (4)$$

The accurate S-values has to be calculated with Monte Carlo simulation program to generate small animal S-values, where the cross dose from the energetic beta particles are considered. Such data can be found in *Hindorf et al* (2).

These dosimetry calculations can be based on the *in vivo* pinhole SPECT measurements described in this work. The results from the measurements to be applied in such analyses and calculations are left for future work.

ACKNOWLEDGMENTS

The author would like to thank supervisor Sven-Erik Strand and Linda Mårtensson, Lars Lindgren and Rune Nilsson at Mitra Medical AB for all practical help and collaboration in the animal studies and John Palmer who has been a great help in problems regarding the scintillation camera and SPECT physics. Thank You!

REFERENCE LIST

(1) Strand SE, Ivanovic M, Erlandsson K et al. Small animal imaging with pinhole single-photon emission computed tomography. *Cancer*. 1994;73(3 Suppl):981-984.

(2) Strand SE, Ivanovic M, Erlandsson K et al. High resolution pinhole SPECT for tumor imaging. *Acta Oncol*. 1993;32(7-8):861-867.

(3) Weber DA, Ivanovic M, Franceschi D et al. Pinhole SPECT: an approach to in vivo high resolution SPECT imaging in small laboratory animals. *J Nucl Med*. 1994;35(2):342-348.

(4) Hindorf C, Ljungberg M, Strand SE. Evaluation of parameters influencing S values in mouse dosimetry. *J Nucl Med*. 2004;45(11):1960-1965.

(5) Schmitt A, Bernhardt P, Nilsson O et al. Radiation therapy of small cell lung cancer with 177Lu-DOTA-Tyr3-octreotate in an animal model. *J Nucl Med*. 2004;45(9):1542-1548.

(6) Strand SE, Lamm IL. Theoretical studies of image artifacts and counting losses for different photon fluence rates and pulse-height distributions in single-crystal NaI(T1) scintillation cameras. *J Nucl Med*. 1980;21(3):264-275.

(7) Deloar HM, Watabe H, Aoi T, Iida H. Evaluation of penetration and scattering components in conventional pinhole SPECT: phantom studies using Monte Carlo simulation. *Phys Med Biol*. 2003;48(8):995-1008.

(8) Beque D, Nuyts J, Bormans G, Suetens P, Dupont P. Characterization of pinhole SPECT acquisition geometry. *IEEE Trans Med Imaging*. 2003;22(5):599-612.

(9) Smith MF, Jaszczak RJ. An analytic model of pinhole aperture penetration for 3D pinhole SPECT image reconstruction. *Phys Med Biol*. 1998;43(4):761-775.

(10) McElroy DP, MacDonald LR, Beekman FJ, Yuchuan W, Patt BE, Iwanczyk JS, Tsui BMW, Hoffman EJ. Evaluation of A-SPECT system for small animal imaging. *IEEE* 0-7803-7324-3/02, pp 1835-1839 2002.

(11) Williams MB, Stolin AV, Kundu BK. Investigation of spatial resolution and efficiency using pinholes with small pinhole angle. *IEEE* 0-7803-7636-6/03, pp 1760-1764 2003.

(12) Hwang AB, Iwata K, Hasegawa BH. Simulation of depth of interaction effects for pinhole SPECT. *IEEE* 0-7803-7324-3/02, pp 1293-1297 2002.

(13) Mird Primer For dose calculations. Revised Edition. 1991. The Society of Nuclear Medicine, Inc.

(14) Hall EJ. Radiobiology for the radiologist. Fifth Edition. ISBN 0-7817-2649-2. Lippincott Williams & Wilkins 2000.

(15) Knoll GF. Radiation Detection and Measurement. Third edition. ISBN 0-471-07338-5. John Wiley & Sons, Inc. 2002.

(16) Xiao S, Bresler Y, Munson DC. Fast Feldkamp algorithm for cone-beam computer tomography. *IEEE* 0-7803-7750-8/03, pp 11-819 – 11-822 2003.

(17) Li J, Jaszczak RJ, Coleman RE. Quantitative small field-of-view pinhole SPECT imaging: initial evaluation. *IEEE Transactions on Nuclear Science,* vol. 42, no. 4, August 1995. pp 1109-1113.

(18) Schramm N, Wirrwar A, Sonnenberg F, Halling H. Compact high resolution detector for small animal SPECT. *IEEE* 0-7803-5696-9/00, pp 1479-1482 2000.

(19) Jaszczak RJ, Li J, Wang H, Zalutsky MR, Coleman RE. Pinhole collimation for ultra-high-resolution, small-field-of-view SPECT. *Phys. Med. Biol.* Vol. 39, pp 425-437, 1994.

(20) Ogawa K, Kawade T, Nakamura K, Kubo A, Ichihara T. Ultra high resolution pinhole SPECT for small animal study. *IEEE Transactions on Nuclear Science,* vol. 45, no. 6, December 1998. pp 3122-3126.

(21) Feldkamp LA, Davis LC, Kress JW, Practical cone-beam algorithm. *J. Opt. Soc. Am.(A),* Vol. 1, pp 612-619, 1984.

(22) Palmer J, Wollmer P. Pinhole emission computed tomography: Method and experimental evaluation. *Phys. Med. Biol.* Vol. 35, no. 3, pp 339-350, 1990.

(23) Garibaldi F, Accorsi R, Cinti MN, Colilli S, Cusanno F, De Vincentis G, Fortuna A, Girolami B, Giuliani F, Gricia M, Lanza R, Loizzo A, Loizzo S, Lucentini S, Majewski S, Santavenere F, Pani R, Pellegrini R, Signore A, Scopinaro F. Small animal imaging by single photon emission using pinhole and coded aperture collimation. *IEEE* 0-7803-8257-9/04, pp 2095-2099, 2004.

(24) Habraken JB, de Bruin K, Shehata M, Booij J, Bennink R, van Eck Smit BL, Busemann Sokole E. Evaluation of high-resolution pinhole SPECT using small rotating animal. *J Nuc Med.* 2001:42(12):1863-1869.

(25) Zeniya T, Watabe H, Aoi T, Kim KM, Teramoto N, Hayashi T, Sohlberg A, Kudo H, Iida H. 3D image reconstruction using complete data in pinhole SPECT. *IEEE* 0-7803-8257-9/04, pp 2100-2102, 2004.

(26) Ishizu K, Mukai T, Yonekura Y, Pagani M, Fujita T, Magata Y, Nishimura S, Tamaki N, Shibasaki H, Konishi J. Ultra high resolution SPECT system using four pinhole collimators for small animal studies. *J Nuc Med.* 1995:36(12):2282-2287.

(27) McKee BTA, Chamberlain MJ, Hewitt TA. A new direction in nuclear medicine imaging: Pinhole Tomography. *IEEE* 0-7803-3312-8/97, pp 1350-1353, 1997.

APPENDIX

SCINTILLATION CAMERA PROPERTIES

The scintillationcamera consists of a 3/8 inch NaI (Tl) crystal coupled to a light guide and photomultiplicator (PM) tubes. The PM-tubes are then connected to electronics and AD-converters. Every event in the crystal representing interaction with incident radiation will generate scintillation light which will generate pulses of different amplitude from all adjacent PM tubes. The PM tube closest to the event will have the highest pulse amplitude and the other surrounding tubes will have degraded pulse amplitude, which magnitude will be proportional to the distance (squared) to the interaction event. The center of light emmitance amplitude is then interpolated from the nearest PM tubes, through a couple of calculation processes to generate the resulting analog signal, which is then digitalized by a fast AD converter and in the end accumulated as a pixel value in a two- dimensional matrix.

The total spatial resolution properties of the scintillationcamera are divided into three parts according to equation 1. The intrinsic resolution, R_i, is governed by the electronics and the detector quantum efficiency, which describes the scintillation light exchange of the multiple interactions in the crystal. The geometrical collimator resolution, R_c, is the dominating part of scintillation camera resolution. The collimator resolution is only dependent on the geometrical properties and the construction of the collimator. The last part, R_s, is due to scattering within the patient or object geometry.

$$R_{tot}^2 = R_i^2 + R_c^2 + R_s^2 \qquad (1)$$

To measure the spatial resolution of a scintillation camera, it is custom to analyze the measured point spread function or the *modulated transfer function* (MTF). This function is the absolute value of the Fourier transform of the point spread function and describes the camera ability to generate an image from modulated information received by the detector from the object. If an infinitesimal narrow beam of photons is exposed to the camera, the scintillation camera would modulate the information and generate a Gaussian profile over the source in the resulting image. This phenomenon is governed by the statistics in the camera electronics and physical interaction properties. The modulation transfer function is a more accurate way to describe the camera resolution.

THEORY OF PINHOLE SPECT IMAGING

COLLIMATOR CHARACTERISTICS

To explain different characteristics of the pinhole collimator, it is convenient to know certain parameters to describe the geometry. The different parameters within the pinhole collimator geometry are illustrated in *figure 1*.

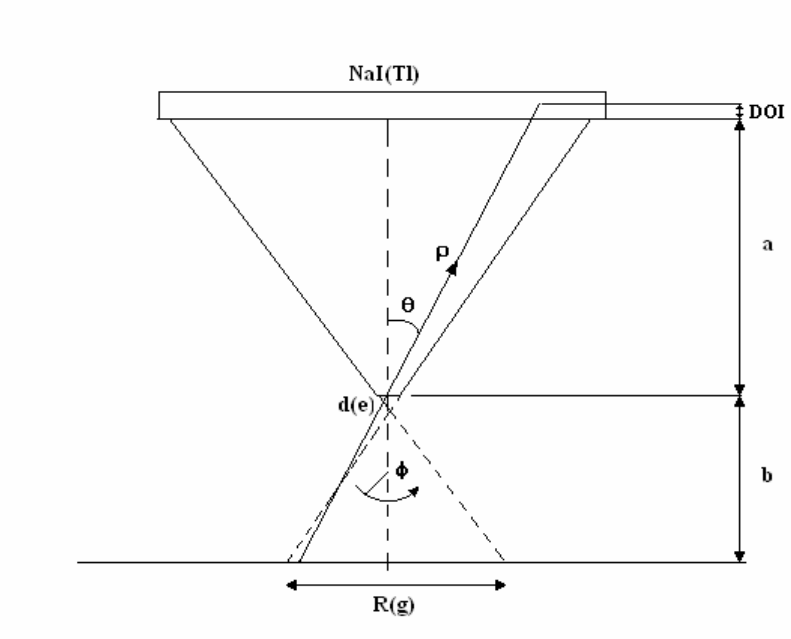

Figure 1. Geometry of the pinhole collimator

To understand the characteristics of the pinhole imaging system, the following parameters in text has to be considered.

The distance from crystal surface and pinhole aperture - *a*, distance pinhole aperture to object – *b* and the radial distance from the center line perpendicular to the surface through the pinhole aperture - ρ, according to *figure 1*. Further on, the smallest distance between two small point sources that the collimator can resolve as two points in the image, denotes R_g. This parameter is commonly measured with a line profile through the image, where "full with at half maximum" (FWHM) is studied.

If we reduce the distance b (see figure 1), the camera axial radius is also reduced and it will result in a better spatial resolution in the image. The resolution and sensitivity for different pinhole-object distances (b) have been evaluated by DP McElroy *et al* (2002). The effect of an increased spatial resolution is thus on cost of a smaller FOV. When distance between the object and the pinhole is reduced, a reduced area of the object is projected against the crystal. This effect is due to the cone formed construction of the collimator.
This phenomenon can be described according to equation 2.

$$FOV \propto \frac{b}{a} \qquad (2)$$

To describe the resolution properties of pinhole collimated scintillation camera systems, a couple of geometric parameters need to be defined. As shown in *figure 1*, θ, ϕ and ρ defines the three spherical space coordinates, where ϕ defines the azimuthally angle and θ represents the angle relatively the central axis of the pinhole collimator.

$$R_g = \frac{(a+b)\cdot d_e}{a} \tag{3}$$

$$R_0 = \sqrt{R_g^2 + \left(\frac{b}{a}\cdot R_i\right)^2 + R_s^2} = \sqrt{\frac{(a+b)^2\cdot d_e^2 + b^2\cdot R_i^2 + a^2 R_s^2}{a^2}} \tag{4}$$

$$d_e = \sqrt{d^2 + \frac{4}{\pi}\int_0^{2\pi} d\phi \int_{d/2}^{\infty} d\rho\cdot\rho\cdot e^{-\mu\cdot\Delta L(\theta,\phi,\rho)}} \tag{5}$$

Equation 3 expresses how the spatial resolution is dependent on the efficient pinhole diameter (d_e), the detector crystal surface to pinhole length (a) and the pinhole to object length (b). The variables d_e and b can be modified to alter the geometrical collimator resolution. The intrinsic spatial resolution, the geometrical collimator resolution and the factor due to scatter in the object are then combined to express the total resolution properties of the scintillation camera system in equation 4. As seen in equation 5 and 6, the effective diameter (d_e) of the pinhole insertion is influenced by the geometrical properties and has a significant part in the geometrical efficiency of the collimator. The pinhole resolution is then to be described through equation 5 (effective diameter) and its geometrical efficiency from equation 6.

Planar imaging with scintillation detector system combined with a pinhole collimator is an excellent instrument to use if small structures within an object are to be imaged. The geometry of the collimator provides a magnification effect of the object. One disadvantage of the pinhole collimator is the reduction of field of view (FOV), which is an effect of the cone formed shape of the collimator. The view that the crystal in the detector head will ”see” is small, compared to other types of detector configurations, that is, other types of collimators i.e. parallel hole collimators. The pinhole collimator has one small hole, which effective diameter (d_e)[v] which sets the crystals view of the object. In exchange of the reduced FOV, the object in the image is magnified.

The camera sensitivity is strongly angle dependent and decreases in radial direction from the collimator central axis as seen when imaging a plane flood source. This angle dependence originates from the geometry of the pinhole collimator. Another effect is the phenomenon of “depth of interaction” (DOI) occurring at locations (according to the probability distribution)

[v] See *figure 1*.and eq. 5.

in line of radiation path. This phenomenon is governed by statistics, in the crystal and blurs or smoothes an image of an object in the edges. This effect is due to the increasing radiation incident angle to the scintillation crystal (10). The angle dependent effect of pinhole collimator is affecting the efficiency and is mathematically described in the equation of collimator geometrical efficiency.

$$g = \frac{\left(d^2 + \frac{4}{\pi} \int_0^{2\pi} d\phi \int_{d/2}^{\infty} d\rho \cdot \rho \cdot e^{-\mu \Delta L(\theta,\phi,\rho)} \right) \cdot \sin^2 \theta}{16 \cdot b^2} = \frac{d_e^2 \cdot \sin^2 \theta}{16 \cdot b^2} \qquad (6)$$

PINHOLE SPECT CHARACHTERISTICS

Pinhole SPECT imaging is a highly suited technology for small animal studies, because of its properties of generating high resolution images over a small volume. SPECT is based on multi angle radiation detection, where the count rate information in every angle is sampled to be used in generating tomographic images of the object containing radioactivity.

To generate tomographic SPECT images of good quality a 360° rotation of the gantry through the rotational plane should be performed to gather enough tomographic information. Information collected in less than 360° is though sometimes performed, but with decreased tomographic image quality because of the less sampled angles.

The gantry is positioned in a specified number of angles to collect projection profiles of the objects activity distribution. These numbers of angles must be chosen to match the dimension of the work matrix in the reconstruction algorithm. The projection profile sampling can be visualized as ordinary pinhole planar imaging, and are sampled in circular plane round the object to gather data to be able to generate tomographic images. The information in every angle is saved in different projection matrices and is then to be used as input data in an iterative reconstructive algorithm. The computer algorithm used in the tomographic SPECT processing system, is a cone beam OSEM iterative reconstruction algorithm.